Research Article

SOHAG JOURNAL OF SCIENCES

https://doi.org/10.21608/sjsci.2023.235198.1122

Development of New Mixed Cu(II) Chelate Based on 2-Benzimidazolylguanidine and Phenanthroline Ligands: Structural Elucidation, Biological Evaluation, DFT and Docking Approaches

Ahmed M. Abu-Dief[1,2], Tarek El-Dabea[1,3], Rafat M. El-Khatib[1], Aly Abdou[1], Mahmoud Abd El Aleem Ali Ali El-Remaily[*,1]

[1] *Department of Chemistry, Faculty of Science, Sohag University, Sohag 82524 Egypt*
[2] *Chemistry Department, College of Science, Taibah University, P.O. Box 344, Madinah, Saudi Arabia*
[3] *Chemistry Department, Faculty of Science, King Salman International University, Ras Sudr, Sinai 46612, Egypt*
**Email: msremaily@yahoo.com*

Received: 9th September 2023 **Revised:** 4th December 2023 **Accepted:** 15th January 2024
Published online: 14th February 2024

Abstract: A new mixed ligand complex with metal ion Cu(II) of the type [Cu(II): HL:P] (where HL = 2-Benzimidazolylguanidine and P = Phenanthroline) was synthesized and characterized using (Ft-IR, Mass, electronic, and NMR) analysis, magnetic moment, thermal studies and stoichiometry analysis Job`s method. Mass spectra for [Cu(HL)(P)(CH3COO)2]H2O complex were studied. Also, pH stability for the CuPL chelate was estimated by employing a spectrophotometric analysis. The observed data revealed that (HL and P) ligands behaved as neutral bidentate ligands with NN donation sites. An octahedral geometry for the CuPL complex was proposed based on spectroscopic data. The thermogravimetric study was used to investigate the metal complex temperature stability and deterioration. A theoretical investigation of the Cu(II) complex was performed with the DFT/B3LYP computational method. DFT calculations better understand molecular mechanisms that could not be elucidated experimentally where the energy gaps and other key theoretical parameters were calculated. The vina dock mechanisms and affinities of Cu (II) complexes for (PDB ID: 3cku), (PDB ID: 2vf5), and (PDB ID: 5IJT), receptors were also investigated. The mixed ligand complex was evaluated for antimicrobial and anticancer efficacy against three species of bacteria, fungi, and cancer cell lines. CuPL complex inferred antimicrobials and anticancer activity against the studied organisms which makes them promising drugs.
Keywords: Guanidine, Phenanthroline, thermo-kinetic, DFT, anti-bacterial, cytotoxicity, molecular docking.

1. Introduction

In comparison to traditional chelates, mixed ligand chelates have at minimum two diverse types of ligands linked with the same metal ion in its salt for the chelation. After a copper metal salt has linked with more than one ligand, this piques the researcher's curiosity in the creation of mixed ligand complexes with a variety of features. The preparation, as well as structure identification of mixed ligand chelates, are becoming increasingly important. Several researchers were concerned in this area due to the growing interest in it [1]. Mixed ligand chelates are recognized in the scientific community to play a significant role in biomedical systems [2]. These chelates were exposed to be physiological agents besides a variety of pathogenic microbial and cancer strains [3]. Bi-dentate ligands are a common type of studied ligand in chelation chemistry, and they have a varied series of usages [3]. Unlike organic reactions for example oxidation, oxidative cleavage, reduction, hydro-formylation, and others, have been discovered to be catalyzed by metal-ligand complexes. In the biological field, mixed ligands play an essential role, as evidenced by the several ways in which metal ions are known to activate enzymes [4]. It is possible to imbue metals with a set of desired properties for particular applications by chelating them with suitable ligands. It is expert through varying features of metal salts like solvophilicity, nucleophilicity, oxidation state stability, and electrophilicity. It may be done by varying the metal and choosing one of the several ligands presented for chelation [4]. Guanidine and benzimidazole reflect a potent nucleus that donates to designing drugs due to their wide therapeutic effectiveness [5]. Mixed coordinating molecules have been obtained from guanidine and benzimidazole derivatives displayed various therapeutic performances like free radicals, bacteria, pain, fungi, allergy, hypertension, cancer, malaria, and inflammation [6, 7] guanidine as well benzimidazole may form ligands were widely working in now years to prepare Metallo Bio site exchanges like (galactose & catechol) oxidase [7, 8], phosphatase [9], urease and many others. A lot of guanidine derivatives have the interesting ability to bind with metal ions to form their respective chelates of the core group, transition metal elements, through their features significantly explained through performance. The growth of stable chelates with various metal salts is due to the lone pair of electrons interacting in its structure [10]. The utilitarian characteristics of these complexes have gotten a lot of attention because of their various applications, involving analytical chemistry, electrochemistry, food, agrochemical, pharmaceutical, and dye industries, and biological fields, because of their structure flexibility, sensitivity well selectivity towards a multiplicity of micro-organisms [10]. Cu(II) is an endogenous metal salt with high anti-microbial and antioxidant activities that are favorable features to be applied as

metallo-drugs [11]. Oppositely, study reports specify that the nature of the tested ligand with the metal chelates is expected accountable for its biological behavior.

The vital medical part of metal chelation molecules of biologically active ligands has appreciated a lot of growth in their genetic applications in recent years [12]. The flexible structure of benzimidazole ligands by (CH2) spacers was taken great attention, which may adopt varied conformations through incomes of the torsional elasticity of its (CH2) spacers to satisfy the complexation request for the core metal in the meeting process [13-15], for designing, developing and formulate imidazole-constructed pharmaceutical agents in an extensive range of biological fields, like, anti-microbial, anti-cancer, and anti-HIV, therapeutic activities have occupied benefit of the imidazole ring's exclusive structural properties as a good electron. Therefore, the attachment for imidazole rings as well a diazo moiety in a lone molecule weight results in the development of compounds with various biological performances as well interesting features. So, maintenance of the study in the azo benzimidazole derivatives has testified to the preparation of six new azo benzimidazole or imidazole derivatives [16]. Herein, the above-studied compounds focus on the interesting suitable biological functionality and great use potential of Cu(II) chelate in bio-medical. So, the area of our present study was prepared and identified CuPL chelate. the spectroscopic classifications as well as analysis of (HL & CuPL) through FT-IR, mass, NMR, UV–vis, and analytical methods besides with DFT study. The studied chelate was screened for in vitro anti-bacterial & and anti-fungi activity against various strains. Moreover, the studied chelate was studied for anti-cancer effectiveness against three cell lines [hepatocellular HepG-2, colon HCT-116, and breast MCF-7] carcinoma. Also, molecular docking is applied for extra support as a promising drug

2. Materials and methods

2.1. Chemicals &Instrumentation

All used solvents, materials, and reagents in this study were supplied from Fluke, Merck, and Sigma-Aldrich and utilized without additional refining. All instruments employed in this work were programmed with supporting information.

2.2 Synthesis of HL ligand

HL ligand was prepared relating to our previous studies in the literature [17, 18]. As shown in (**Scheme 1**)

2.3 Synthesis of CuPL chelate.

Cu(II) mixed ligand chelate was prepared by dissolving 20 mmol of Copper acetate in a suitable amount of EtOH. After that, the equimolar amount of the HL ligand (20 mmol) and Phenanthroline (P) ligand (20 mmol) were dissolved individually in 10 mL of EtOH through heating. The ethanolic solutions of HL ligand were firstly added dropwise to Cu (II) and refluxed for 30 minutes then (Phen) ligand was added dropwise to the refluxed solution. The total solution gives equal molar for the (HL & P) ligands in chelation to the metal salt. The resulting mixture was refluxed for 2 h to complete the reaction; the obtained product was precipitated on hot, filtrated & and purified with hot (EtOH), respectively. As shown (**Scheme 1**)

2.3 TGA study

TGA analysis proposes to evaluate the hydrating nature and the dehydrating nature of the tested chelates which relates to the presence as well the absence of H_2O molecules, respectively. The study has been prepared through solid material below N_2 with the ratio of heating (5°C min^{-1}) in addition to a wide range of temperatures (50:800°C).

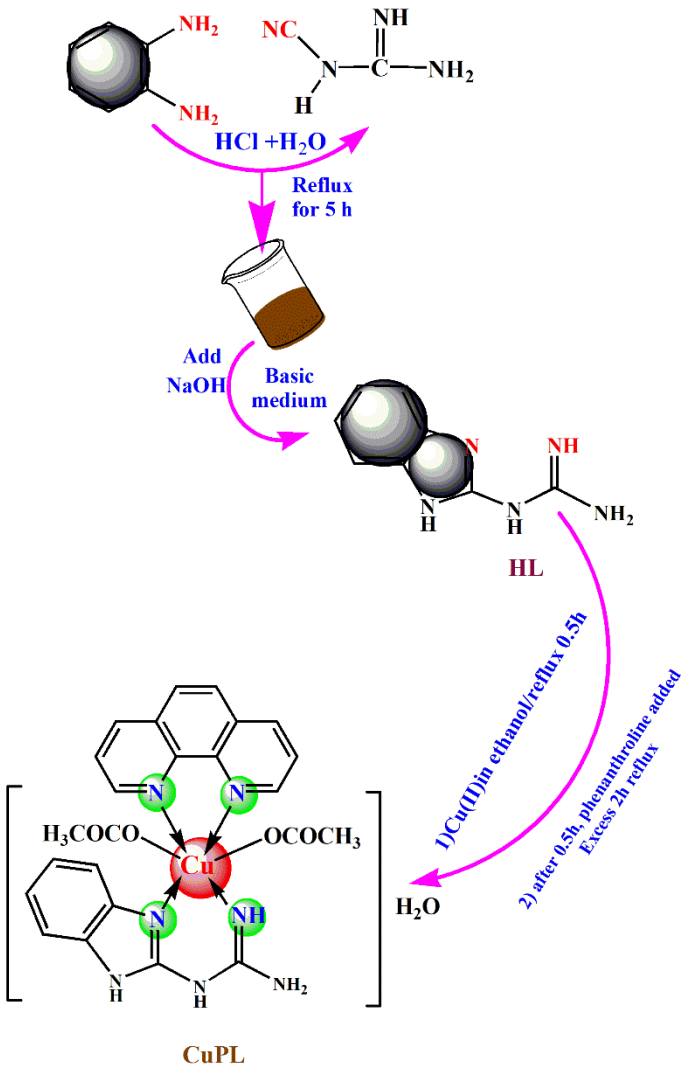

Scheme 1: Preparation of HL ligand and CuPL mixed complex.

The degradation curve for the titled chelate was limited to four steps that have been started around 45°C. The resulting stages are accomplished for broad alteration to the title chelate. The minor thermal stability of the titled chelate shows the occurrence of H_2O molecules which was recommended earlier. Thermo-kinetic parameters were estimated through known relations [19-20]. Like [Coats-Red fern as well Horowitz-Metzger] relations [21].

2.5. Stoichiometry and Formation CuPL complex

The stability and stoichiometry of mixed ligand chelates were examined through Ligand exchange & and job's method in solutions [22-23]. The absorbance was evaluated for the related addition of both (CuL & and P).
Then, the mixture was sonicated for 10 minutes as well to balance for all tested solutions, The resultant absorbance in the tested solution was charted vs. the ligand and metal mole fractions ([P]/[P]+[CuL]), and the ligand to metal molar ratio ([P]/[CuL]). The formation constants (K_f) of the CuL chelate have been done through spectra study towards the next relative [22]; $Kf = AAm/(1-A/Am)^2C$. Wherever, [Am], [A] & [C] was the maximum absorbance for transmittance bands, the transmittance data beside each side of absorption bands that casually allotted, and the molar dose of the studied metal, respectively. As well, ΔG* results [free energy changes] have been estimated through the next calculation [ΔG= -RT Ln Kf] (at 25°C). Wherever, [R], [Kf], and [T] are the constant of gas, the constant of formation, and the temperature in kelvin respectively [23].

2.6. Electronic study

The electronic spectra of the studied chelates have been recorded at 298 K in DMSO solvent, for studying the UV-Vis wavelengths in between 200:800 nm.

2.7. Computational methodology

Utilizing hybrid DFT/B3LYP [24] at the 6-311G (d, p) level for the free ligand and LANL2DZ level for the metal atoms, the initial molecular geometries of the ligand and metal complexes were optimized [25]. To study global reactivity features, such as energy gap, hardness, softness, electrophilicity, and electronegativity, the energies of the highest occupied molecular orbital (HOMO) and the lowest unoccupied molecular orbital (LUMO) were employed. HOMO stands for highest occupied molecular orbital, while LUMO stands for lowest unoccupied molecular orbital [26].

2.8. Docking technique

A model of ligand-protein interaction was built with the help of Molecular Operating Environment (MOE). The glucosamine-6-phosphate synthase of Escherichia coli (PDB ID: 2vf5) [27], the urate oxidase of Aspergillus flavus (PDB ID: 3cku), and the Human Peroxiredoxin 2 Oxidized (SS) (PDB ID: 5IJT), have been downloaded from the Protein Data Bank (http://www.rcsb.org/pdb). Several procedures were carried out to repair the protein before docking. These procedures included removing solvent molecules and co-ligands, adding hydrogens, repairing the chain, and choosing active sites. In addition, the compounds that were put to the test underwent an optimization process for docking that included the reduction of energy, energy adaptation, calculation of atomic charge, and calculation of binding energy. In this area of research, the stability of H-bonds and van der Waals adducts may be determined by analyzing a diverse set of structures [28, 29]. From a total of thirty different ligand-receptor poses, five conformers were chosen that each represented the ligand molecule that could be implanted into the protein active pocket with the least amount of rotation and the highest scoring energy. The binding free energy and hydrogen bonds that exist between the ligand and the amino acid were considered while performing the calculation used to rank the ligand's and metal complexes' affinity for the target protein [30].

2.9 In Vitro Anti-microbial Assay.

Anti-microbial analysis for the studied compounds presented in this study has been inspected against numerous microbial strains employing the diffusion agar procedure [31]. The microbial strains utilized to analyze the anti-microbial performance are the G (+ve) bacteria (B. subtilis), the two G (-ve) bacteria (E. coli & S. Typhimurium), and the fungi strains (A. flavus & F. oxysporum & G. candidum). The anti-microbial study was estimated as a mean of three times [31]. [MIC] minimum inhibitory concentration has been evaluated as well as definite as the minimum treatment dose that avoids growth through 50% [32]. The full method for the anti-microbial study is declared in the supporting data (**Part S2**)

2.10 In Vitro Cytotoxicity Assay.

In vitro, the anti-tumor performance of the studied chelate in this study has been inspected employing the standard MTT process [33]. The cell lines used to estimate the action are (HePG-2 & MCF-7 & and HCT-116). The MTT analysis is a reference colorimetric study that is applied to estimate cell growth. It is applied to estimate the cytotoxicity of probable therapeutic agents. The obtained IC_{50} data have been voiced as the mean value ± (SD). The full method for the MTT analysis is declared in the supporting data (**Part S3**) [34].

$$IC(\%) = \frac{control_{OD} - compound_{OD}}{control_{OD}} \times 100$$

3. Results and discussion

3.1 General properties

The data observed through the physical and analytical study verified the recommended chemical formulae for CuPL chelate. The stoichiometric relation for the colored CuPL chelate was (1 Cu: 1HL: 1P, **Scheme 1**) as demonstrated through the DFT study. The studied CuPL chelate was soluble only in DMSO & and DMF, stable in air, and non-hygroscopic. There was a good agreement between CHN micro-analyses, TGA, mass spectra, and the chemical formulae suggested. The obtained conductivity value of CuPL chelate (15.16 $\Omega^{-1}cm^2mol^{-1}$) exhibited its non-electrolytic property and the magnetic moments specified that the CuPL chelate has a paramagnetic property. This data is represented in (**Table 1**)

3.2. IR & NMR analysis

KBr-discs were set for the HL & IR compounds to examine the changes that occurred to lower the influence of the radiation of IR done the functional groups [35]. The HL ligand displayed vibrations of (N−H), and (C=N) at 3419 and 1640 cm^{-1}, respectively. Comparing the spectra of CuPL chelate (**Figure S1**) through that of the HL ligand has suggested a result around the binding approach in the CuPL chelate. Significant changes were detected for υ(N−H), and (C=N) vibrations in the HL ligand, due to its chelation through the metal ions. The tested

ligand acted as a bi-dentate toward the metal ions. Finally, the new peaks detected around 470 and 534 cm^{-1} could be apportioned towards the vibration of υ(M−N) & υ(M−O) in CuPL chelate [17, 38] as shown in (**Figure S1 and Table 1**). ^{1}H & ^{13}C NMR study for HL was done in DMSO-d6 solution as exposed in our previous studies in the literature [17] as shown in (**Figures S 2, S 3**)

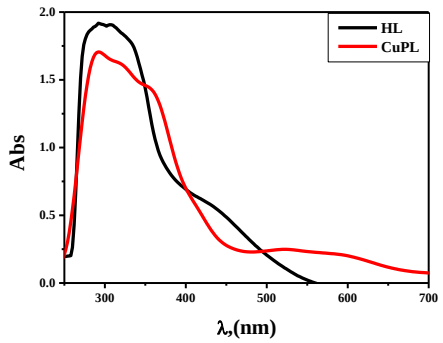

Fig. 1: Electronic spectra of HL ligand and its Mixed Cu chelates in DMSO [$1x10^{-3}$] M at 298K.

3.3 Optical characterization

To obtain UV–Vis electronic transitions in the chemical structure, these tested compounds can be dissolved in DMSO for the trace quantity. Now, HL and CuPL compounds were dissolved in DMSO on cold and using ultrasonic and then scanned at 200:800 nm. The ligand field d−d transitions, charge transfer (CT), n→π*, π →π* as well as intra-ligand transitions have been documented (**Figure 1**) to study the geometry of chelation of CuPL complex. The electronic transitions involved in the HL ligand and CuPL chelate have been documented in DMSO over the scale of 200: 800 nm. The studied ligand displayed absorption peaks of about 293 nm due to the (π→π*) transitions. Besides, the absorption peaks seeming around 308 nm are caused by the presence of (n→σ*), also a peak appeared around 447 due to the (n→π*) transitions. These observed peaks suffered from a shift in wavelength due to the chelation. The electronic absorption spectrum of the Cu(II) complex shows a broad band around 523 nm can be attributed to LMCT transition and a band around 601 nm can be attributed to $^{2}Eg \rightarrow {}^{2}T_2g$. The broadness of the band is due to the ligand field effect and the Jahn-Teller distortion of the metal complexes. These absorptions confirmed the distorted octahedral geometry around Cu(II) ions. Moreover, the magnetic moment for the Cu(II) complex is 1.88 B.M. which is within the expected value and establishes the presence of one electron in its outermost shell the d^9 (t_2g^6 eg^3) electron configuration. All visible transitions have been occupied (nm) and then reformed to its wavenumber data (cm^{-1}) (**Table S1**), One of the best ways to figure out the internal structure of metal complexes is to calculate their effective magnetic moment [36]. By calculating the molar susceptibility of the coordination compound and applying diamagnetic corrections for the other ions or molecules in the mixture, one may determine the susceptibility of a paramagnetic metal ion per atom in a certain material [37]. More specifically, the linkages and equations below can be used to compute magnetic susceptibility and effective magnetic moment:

$$\mu_{eff} = 2.83\ [(Xg * Mwt) - (dia\ magnetic\ correction * T)]^{0.5}$$

Where T is the absolute temperature (K), μ_{eff} is the practical magnetic moment (B.M), X_g is the obtained gm magnetic susceptibility, X_M is the molar magnetic permeability before correction, and X_A is the molar magnetic permeability after correction. Bands at 523 nm can be attributed to $^{2}B_1g \rightarrow {}^{2}A_1g$ transitions in the electronic spectra of the Cu(II) complex, suggesting an octahedral geometry centered on Cu(II). In addition, the μ_{eff} of the CuPL complex was measured to be 1.88 B.M, which is consistent with a return to the d^9 (t_2g^6 eg^3) electron configuration. The octahedral geometry may be represented by these values [29]. Various spectroscopic approaches could potentially be exploited to solve the paradox and disclose the true 3d arrangement of these complexes [36, 37].

Table 1: Studied compounds, empirical structure, melting points, abbr, CHN, as well FT-IR bands.

Compound		HL Ligand Reff [17]	CuPL chelate
Color		Pale Brown	Dark greenish blue
M.P (°C)		245	>320
Empirical formula (Formula weight)		$C_8H_9N_5$ (175)	$C_{24}H_{25}N_7O_5Cu$ (554.5)
Magnetic moments		-	1.88
Analysis: found	**N(%)**	39.87 (40.00)	17.80 (17.67)
	H(%)	5.22 (5.14)	4.42 (4.50)
	C(%)	54.73 (54.85)	52.04 (51.93)
IR Cm^{-1}	**υ (NH)**	3419	3437
	$\upsilon(NH_2)$	3273,3185	3336, 3127
	$\upsilon(CH)_{ar}$	3053	3005
	$\upsilon(C=N)\&(NH)_{Im}$	1640,1591	1688, 1650
	υ(M-N)	-	470
	υ(M-O)	-	534

3.4 Mass spectra

The indication of mass spectral study is developing in failure of separating single crystal for the tested chelate. The stoichiometry structure of the CuPL chelate has been related through their mass spectra. **Figure 2** exposes the mass spectra of the CuPL chelate through an enhanced beam of electrons around 70 eV, by heating rate 40 °C/min as well-done mass/charge choice between 50: 800. The following degradation peaks have been estimated on the exhibited patterns to explain the structure formulae for CuPL chelate. The molecular ion [M^+] peak completed in the pattern was 554.70 (calcd. 554.5), for CuPL chelate. The [M^+] molecular ion peak of the Cu(II) complex structure might be assigned to approve the proposed formula of the tested chelate. The additional peaks in the mass

spectrum matched to distinct metal chelate composition. The molecular weights of the studied compounds have been matched with TGA, and CHN to approve the recommended structure and formulae.

The obtained results presented the chelates stoichiometry have been [ML] type. As displayed in (**Figure 2)** [38].

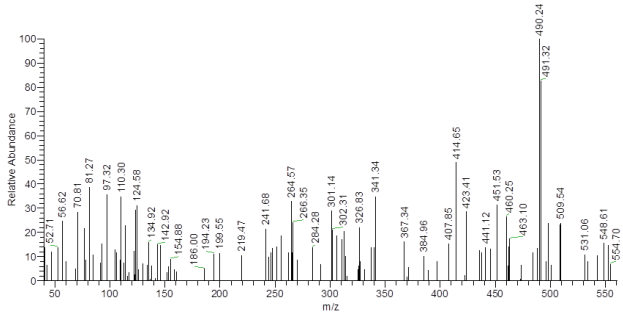

Figure 2: Mass spectroscopy of CuPL chelate.

3.5 Thermal study

The thermal study is a significant and effective process for estimating thermal stability, ordering crystallization substances, and identifying chemical structures. The thermal study has been applied at a 5°C/min heating rate below N_2 atmosphere from 25-800 °C. The detected and the planned data of TGA bands have been collected in (**Table S2, Scheme 2, and Figure. S 4)**. CuPL complex by its chemical formula [Cu(HL)(P)(acetate)$_2$]. H_2O has been thermally degraded through four steps. The first stage evaluated weight loss of 3.29 % (calc. weight loss = 3.24%) between 48 °C to 116 °C which can relate to [H_2O] loss. The next stage with evaluated weight loss of 53.70 % (calc. = 53.73 %) between 118 °C to 380 °C could relate to $C_{16}H_{14}N_2O_4$ molecule loss. The following stage evaluated weight loss of 10.50 % (calc. = 10.45 %) between 382 °C to 560 °C which could relate to CH_4N_3 molecule loss. The next stage with evaluated weight loss of 21.14 % (calc. = 21.09 %) between 562 °C to 720 °C could relate to $C_7H_5N_2$ molecule loss. Finally, the residue has been detected as Cu metal with an evaluated weight loss of 11.33 % (calc. = 11.45%). The overall weight loss is 99.96 % (calc. = 99.96%). In continuance of the thermal study, the thermo-kinetic factors of the degradation stages for the tested chelate were summarized in **(Table S2)** as well as evaluated through the Coats–Redfern & Eyring equations and Horowitz–Metzger analysis [27, 39, 40]. From the observed results, the resulting explanations may be completed.

• The (+ve) results for ΔH* refer that the degradation methods are endothermic.

• The (+ve) results of ΔG* for the studied chelates exposed important growth for the following degradation steps due to the growing values for TΔS* starting from one stage to another one, which directed the results data of ΔH*.

• The ΔS* results of the tested chelates have been established to be (-ve). This means that the stimulated chelate has been ordered more than the started reactants or that that reaction was not fast. [41]

All steps of degradation have been non-spontaneous behavior relating to positive ΔG results. [42] (**Scheme 2, Figure S 4 and Table S2**).

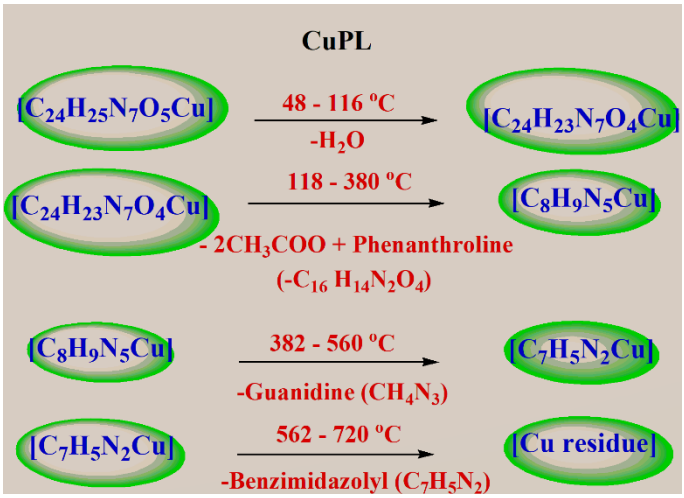

Scheme 2: Themo gravimetric degradation steps for CuPL complex.

3.6. Apparent formation constants, Stoichiometry, and pH profile of complexes

To demonstrate the use of the stepwise Phenanthroline, HL, and Cu(II) reduction behavior, we then discovered efficient ligand exchange responses between studied (Phen & HL) ligands for Cu(II) metal cation. Data display that, once (Phen) has been added to CuL (Cu(II) & HL) (1:1) solutions, the structure of the tested mixed chelates has been evaluated through various systems. Job's system has been applied to evaluate the ratio of HL to Cu(II), and curves applied for the estimation of the ratio of Phen to CuL. The stoichiometry of the studied chelate was presumed from their CHN analysis (**Table 1**), which specifies that the formation of (1: 1: 1) (Cu: HL: Phen) ternary chelate ratio which definite through the solution study relating molar ratio & continuous variation process. As displayed (**Figures. 3 & S 5**), maximum absorbance in the graph has been noticed at (mole fraction, X= 0.5) relating to (1CuL:1P) ratio. The molar parts of the two tested components have been mixed always, observing their shared dose constant as well keeping the other studied component in a great continuous excess towards all tested solutions in the series. The pH estimation has been applied for methods enclosing 1:1:1 molar ratios of the (HL, Phen, Cu(II)). More valuable data has been obtained from the used Cu(II) metal cation that the chelate classes formed have been soluble upon a large scale of pH= 4:10. In the region below pH 5 we observed acid hydrolysis for the prepared complexes leaving ligand and metal chloride. Above pH 10, we observed that the investigated complexes undergo base hydrolysis to afford the ligand and metal hydroxide. As shown in **(Figure 4).** The Kf stability constants for the studied Cu(II) chelate are calculated as (3.33 x 10^5). The data obtained in an ethanolic solution is in good agreement with data documented in the literature [8, 20, 21]. A comparison of the observed results in **(Table 1)** specifies that Cu(II) chelates are expressively more stable than binary chelates having the related stoichiometry. This can be affected by the fact that tested ligands perform as bi-dentate ligands, all of which form fused ring systems. Due to

negative Gibbs free energy that equals.

[**Δ(G*)=-30.8 K.J.mol^{-1}**], the reaction between Cu(II) metal cation and (HL&P) ligands was desirable and spontaneous [43, 44].

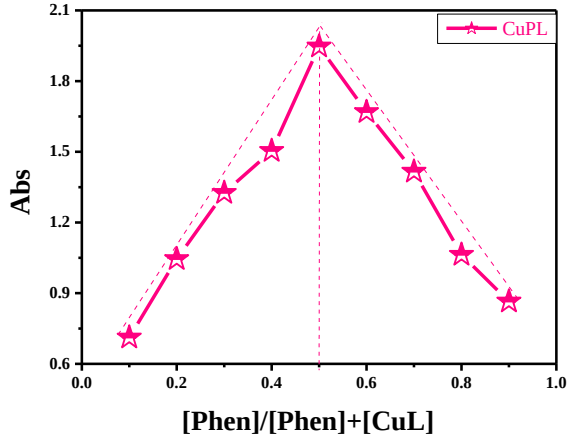

Fig. 3: Curves of continuous variation method for CuPL complex (10^{-3}M) in DMSO at 298 K

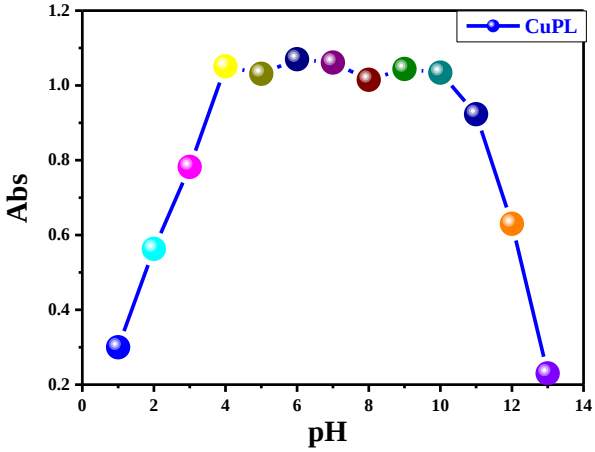

Fig. 4: Dissociation graph of the CuPL complex in aqueous alcohol mixtures at [CuPL]= 1x10^{-3} M and 298 K

3.7. DFT calculation

3.7.1. 3D geometry optimization

Figure 5 depicts the three-dimensional structures of the HL ligand and the Cu(II) mixed complex that it forms in their optimal states. The optimization of the CuPL complex led to the formation of an octahedral geometric structure around the core of the Cu(II) metal cation [**17, 45**].

3.7.2. HOMO-LUMO & global reactivity

The DFT approach was used for each calculation that was performed. One can characterize the three-dimensional structure of the compounds that have been investigated by making use of molecular structures that have been optimized via the use of theoretical approaches. A molecular orbital analysis was performed on the optimized geometries at the levels of DFT/B3LYP (6-311G (d, p) and LANL2DZ), as shown in **(Figure 6)**. On the optimized geometries shown in **(Figure 5)**, investigation into the HOMO-LUMO orbitals shown in **(Figure 6)** and the molecular electrostatic potential (MEP) shown in **(Figure 7)** was carried out. In addition, the frontier molecular orbital energies were used to calculate quantum mechanical descriptors such as the energy gap (ΔE = LUMO - HOMO), ionization energy (IE = -HOMO), electron affinity (EA= -LUMO), electronegativity (EN = (IE+EA)/2), chemical potential (CP = -(IE+EA)/2), chemical hardness (CH = ((IE - EA)/2), chemical global softness (S = 1/2CH), electronic charge (Nmax = -CP/CH), and electrophilicity index (EP = CP2/2CH),[**45, 46**] **(Table 2).**

It was found that the HOMO and LUMO energies of both the HL ligand [**17**] and the CuPL complex had negative values, which indicated that the compounds were stable. The chemical properties that are laid forth in **(Table 2)** give the impression that the metal complex is more active than the free ligand, and the energy gap (ΔE) in all the Cu (II) complex is less than that in the HL ligand [**47**]. This makes the entire metal complex more reactive and stable than the free ligand [48]. In addition, molecular properties that are reliant on electron density, such as electronegativity, and electrophilicity, demonstrate that the Cu (II) metal complex has greater values than the HL ligand does [**48**]. It was hypothesized that the activity of the CuPL complex would be higher than that of the HL ligand. This is because their levels of electronegativity and electrophilicity are higher than those of the HL ligand. As shown in **(Table 2).** In addition, the degree to which a material is hard or soft may have an impact on the extent to which it reacts chemically. This is because hardness and softness are often inversely related. It is possible to understand its reactivity by using an approximation that is known as the hard-soft-acid-base (HSAB) model [**48**].

This model has the potential to be used. Although this is just an approximation, weak acids coordinate with weak bases, whereas strong acids interact with strong bases. Because biological components such as cells and enzymes have soft structures, biological systems interact more favorably with soft chelates. This is because soft structures are more compatible with the soft structures of biological components. This is since the structure of biological components is more comparable to the structure of soft structures. For instance, the degree of biological activity of chelates will increase in direct proportion to the softness degree of the material. Because the chemical potential of each molecule had a negative value, it was claimed that all coordination events are of the spontaneous kind.

The octahedral geometry of the Cu(II) complexes also can be confirmed from the optimized 3D geometry resulting from the DFT calculations, especially, from the bond-angles values around the Cu(II) center. Where the octahedral shape is characterized by octahedral bond angle values of 90° and 180°. The angle between the four atoms forming the square base of the two pyramids in the octahedral structure is 90°, as is the angle between any of those atoms and either of the vertex atoms. From the bond-angles values around the Cu(II) center, the following Table, these values are comparable to that of the standard octahedral geometry, which confirms the octahedral geometry around the Cu(II) center in the Cu(II) complex As shown in **(Table 3).**

HL

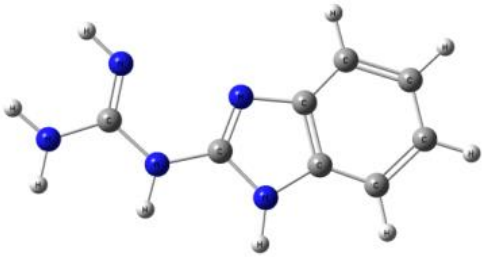

CuPL

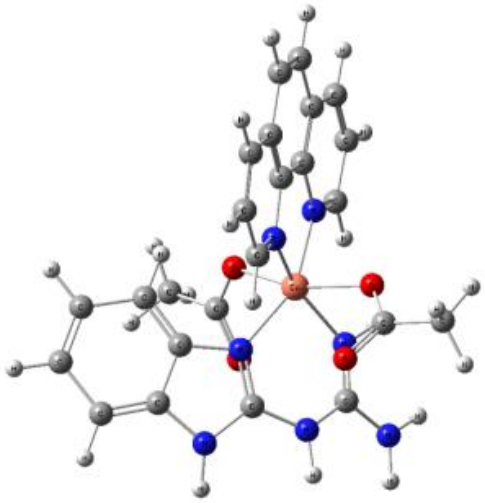

Fig. 5: the conformation structure of the studied compounds

3.7.3. Molecular Electrostatic Potential (MEP)

The physicochemical properties and the molecular structure of a molecule are both related to its molecular electrostatic potential (MEP). (**Figure 7)** maybe used to display the MEP for the chemicals that were under investigation. Red and blue in MEP stood for the negative region for electrophilic attack and the positive region for nucleophilic assault, respectively. The neutral area was identified through the green hue. A reddish negative zone surrounds the nitrogen atoms as the potential rises from red to green to blue. As a result, it can be concluded that nitrogen atoms are the most vulnerable to electrophilic attack [**49**]. Red, green, and blue have the highest potential. it can be concluded that nitrogen atoms are the most vulnerable to electrophilic attack [**49**]. Red, green, and blue have the highest potential.

3.8. MOE-docking simulation

Through estimating the various forms of interaction as well as the binding affinities, an MOE-docking study might potentially provide a more in-depth acceptance for how efficiently novel drugs apply bioactivity against a target [**49**]. A docked chelate, which was estimated based on docking scores, was studied agreeing to binding interactions between the HL ligand and Cu (II) complex with the target protein. This study was carried out through the glucosamine-6-phosphate synthase of Escherichia coli (PDB ID: 2vf5), the urate oxidase of Aspergillus flavus (PDB ID: 3cku) [**50**], and the Human Peroxiredoxin 2 Oxidized (SS) (PDB ID: 5IJT) [**51**] as the targets. The docking analysis demonstrated that the compounds that were prepared feature non-covalent interactions, like ionic, and hydrogen bonding interactions. This information can be found in. The studied chelates, regardless of their docking score levels, showed promising outcomes when linked with the target proteins. In general, the docking site is more stable and the interaction between the docking site and protein receptor is stronger when the energy value (S) is more negative values [**50, 51**].

Table2: Calculated quantum chemical parameters

compound	HL	CuPL
E_{HOMO}	-5.65	-7.80
E_{LUMO}	-0.30	-5.55
IE	5.49	7.80
ΔE	5.35	2.25
EA	1.23	5.55
EN	3.36	6.67
CP	-3.36	-6.67
CH	2.13	1.13
S	0.24	0.44
EP	2.65	19.78

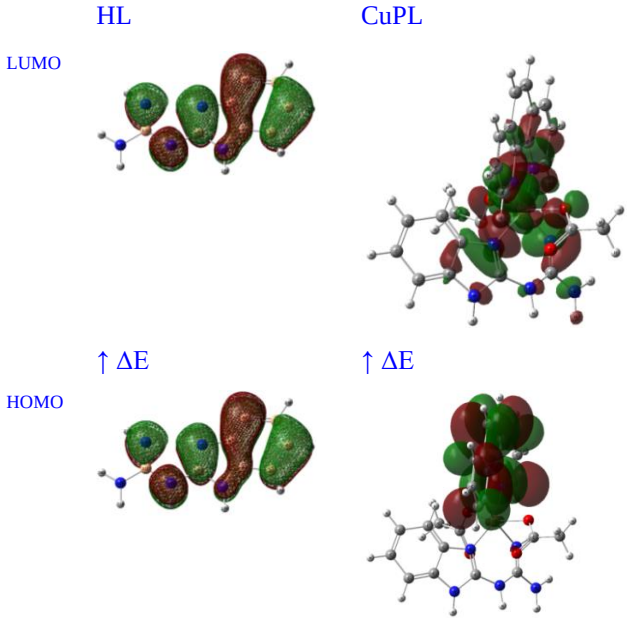

Fig. 6: HOMO-LUMO of the studied compound

Table 3: The most important bond angles around the Cu(II) center in the Cu(II) complex

Angle	Value
N_p-Cu-N_p	87.20277
N_p-Cu-O_{ac}	104.83332
N_p-Cu-O_{ac}	80.20318
N_p-Cu-N_L	89.60028
N_p-Cu-N_L	153.60289
N_p-Cu-O_{ac}	69.47792
N_p-Cu-O_{ac}	90.36621
N_p-Cu-N_L	153.49002
N_p-Cu-N_L	102.37818
N_L-Cu-N_{ac}	86.00612
N_L-Cu-N_{ac}	114.99725
N_L-Cu-N_L	92.01371

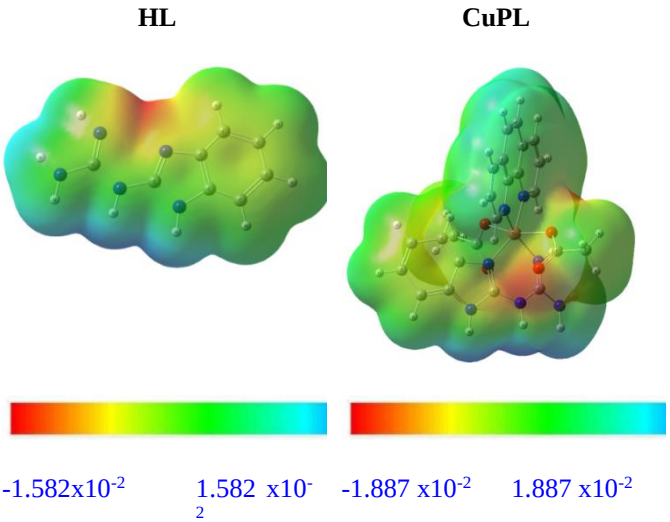

Fig. 7: MEP of the tested compounds

In the case of 2Vf5 protein, **(Table 4)** and **(Figure S6)**; the estimated docking score of the HL ligand was determined at -4.52 kcal/mol [17]. The estimated binding score of the CuPL complex, on the other hand, was calculated at -8.48 kcal/mol. When compared to the HL ligand, the results showed that the CuPL complex had much higher docking scores. Because of this, the binding affinity of the HL ligand is improved thanks to the CuPL complex formation. The HL ligand formed one H- H-acceptor bond with the following amino acid residues: N9 with ASN652, with bond distances of 2.86 Å. The CuPL complex formed four H-donor bonds via N46, N48, N48, and N49 with VAL567, ASP548, VAL567, and ASP548, respectively, with bond distances of 2.84, 2.81, 2.75, and 3.00 Å, respectively. Moreover, the CuPL complex formed two ionic interactions via N43, and N45 both with GLU569, with bond distances of 3.68, and 3.87 Å, respectively, in addition to one pi-H interaction between 6-ring and ASN522 with a distance of 4.22, **(Table 4)**

Table 4: MOE- docking results of the studied compounds as well as the 3cku

Comp.	Ligand	Receptor	Interaction	Distance	E (kcal/mol)	S (kcal/mol)
HL	N 7	GLU 259	H-donor	2.92	-3.30	-4.52
CuPL	C27	GLU 259	H-donor	3.05	-1.00	-8.34
	N48	GLU 259	H-donor	2.86	-5.10	
	N49	GLU 259	ionic	3.23	-3.10	
	6-ring	LEU 170	pi-H	4.59	-0.70	
	5-ring	LYS 171	pi-H	4.31	-0.70	
	N31	GLU 259	ionic	3.09	-3.90	
	6-ring	GLU 259	pi-H	4.44	-1.00	
	5-ring	GLY 272	pi-H	3.73	-1.80	

The calculated docking score for the studied ligand [17] with 3cku protein was evaluated at [-4.52 kcal/mol] **(Table S3)** and **(Figure 8)**. The valued binding score for the CuPL complex was calculated at [-8.34kcal/mol]. Once matched to the tested ligand, data showed that the studied complex had much higher docking scores. Because of this, the binding affinity of the free ligand is improved thanks to the metal chelate formation. More specifically, The HL ligand formed one H-donor bond through the subsequent amino acid residues: N7 with GLU259, with bond distances of 2.92 Å. The CuPL complex formed two H-donor bonds via C27, and N48 with GLU259, with distances of 3.05, and 2.86 Å, respectively. Moreover, the CuPL complex formed one ionic, and two pi-H interactions between N49, 6-ring, and 5-ring with GLU259, LEU170, and LYS171, with distances of 3.23, 4.59, and 4.31 Å, respectively, **(Table S3)**.

The calculated docking score of the tested ligand [17] with 5IJT protein was determined at [-4.66 kcal/mol] **(Table S4)** and **(Figure 9)**. The estimated binding score of the CuPL metal complex was calculated at -8.66 kcal/mol. Once matched to the tested ligand, data showed that metal complexes had much higher docking scores. Because of this, the binding affinity of the free ligand is improved thanks to the metal complex formation. More specifically, comparing the CuPL complex with a docking score of [-8.18 kcal/mol]. The free HL ligand formed one H-donor bond between N12 with GLU170, with a bond distance of 2.91 Å **(Table S 4)**.

3cku
HL

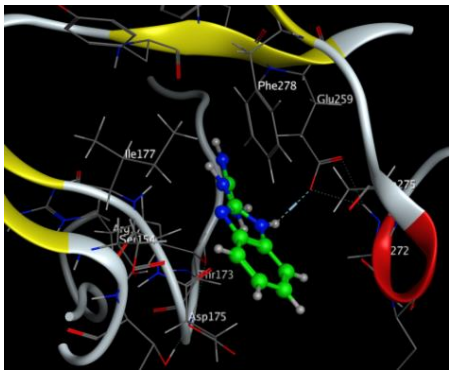

CuPL

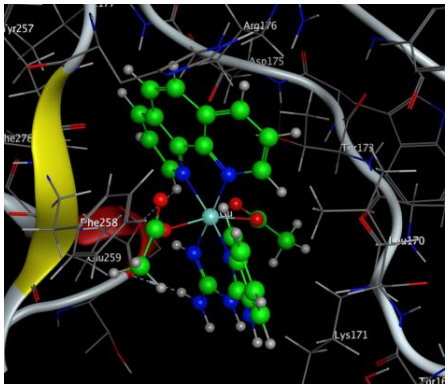

Fig. 8: 3D interactions between the studied compounds and the 3cku

5IJT
HL

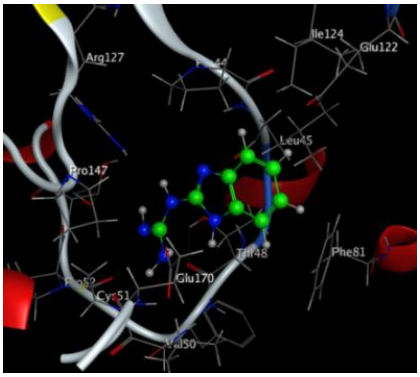

CuPL

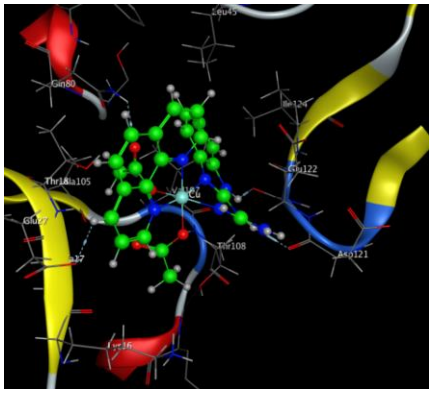

Fig. 9: 3D interactions between the title compounds and the 5IJT

3.9 Anti-microbial activity

All the tested compounds CuPL complex and HL ligand [17] have been tested for their anti-microbial performance against chosen organisms, involving G(+) bacterial strain (B. subtilis), G(-) bacterial strains (E. coli, S. Typhimurium), in addition to fungi, involving (A. flavus & F. oxysporum & G. candida). Data have been calculated in cycles of the zone of inhibition at both 15 and 25 g/ml doses for the studied compounds and also documented as MIC and activity index data in **(Table 4 & 5 & S5 and Figure 10)**. Ofloxacin and Fluconazole have been applied as positive anti-microbial controls. The data display the absence of anti-microbial performance for the HL ligand [17] at the used dose versus selected microbes. Also, the studied CuPL complex has extremely good action versus the examined Fungai & and bacterial strains. Interestingly, the inhibition zone diameters of the CuPL chelate are higher for G(-) bacteria related to the G(+) bacteria.

The inhibition zone diameters for CuPL chelate are 31.85, 25.7, and 42.85 mm against S. Typhimurium, E. coli, and B. subtilis, respectively. Equally, the inhibition zone diameters for ofloxacin are 35.20, 29.2, and 47.1 mm, respectively. The best MIC data were detected for the CuPL chelate against various microbial strains. Commonly, the studied CuPL complex might be believed as a wide variety of anti-microbial agents [51]. Also, metal cations are therefore easily adsorbed on the surface of the cell wall of the organisms and able to disrupt the respiratory process of the cells and block protein synthesis and consequently, limit the additional growth of organisms. Besides this, the substituent methyl group plays a vital role in increasing the lipophilic nature of the metal complexes and is the reason for remarkable antibacterial activity, and other factors like coordinating sites, the geometry of complexes, steric, concentration, and hydrophobicity have considerable influence on the anti-microbial potency. Furthermore, the mixed-ligand technique is pleasurable because of its design which allows different functional groups with variable binding sites and tightly binds to the metal cation forming stable mixed-ligand complexes. The higher antimicrobial activities of the metal complexes compared to the studied ligands may be due to the changes in structure that occur due to coordination and chelation that causes the metal complexes to act as more powerful antimicrobial agents, thus killing the microbe or by inhibiting multiplication of the microbe by blocking their active sites. Such increased activity of the complexes can be explained based on the Overtone concept and the Tweedy chelation theory [**52**]. According to the Overtone concept of cell permeability, the lipid membrane surrounding the cell favors the passage of only lipid-soluble materials, due to which lip solubility is an important factor controlling the anti-microbial activity. On chelation, the polarity of the metal cation will be reduced to a greater extent due to the overlap of the ligand orbital and partial sharing of the positive charge of the metal cation with donor groups. Furthermore, the mode of action of the compound may involve the formation of a hydrogen bond through the azomethine group with the active center of cell constituents, resulting in interference with normal cell processes.

Due to the presence of an electron-withdrawing group in the ligand, the positive charge of the copper ion increases, and this enhances the ability of the copper ion to interact with DNA [**45**]

Table 4: Inhibition zone of anti-microbial assay for CuPL chelate against various strains of (bacteria and fungi).

Compounds		Inhibition zone (mm)± SD		
Conc.(µg/ml)		CuPL	Ofloxacin	Fluconazole
S.Typhimurium (-ve)	15	14.75 ±0.18	18.60±0.15	-
	25	31.85±0.12	35.20±0.12	-
Escherichia Coli (-ve)	15	14.65 ±0.05	17.2±0.14	-
	25	25.7±0.11	29.2±0.15	-
Bacillus cereus (+ve)	15	22.7±0.14	26.40±0.18	-
	25	42.85±0.07	47.1±0.15	-
Aspergillus Flavus	15	13.5±0.04	-	16.35±0.17
	25	22.6±0.18	-	26.45±0.03
Getrichm Candidum	15	22.15±0.16	-	25.15±0.06
	25	39.7±0.07	-	43.35±0.16
Fusarium Oxysporum	15	14.9±0.12	-	18.25±0.19
	25	26.85±0.13	-	31.35±0.07

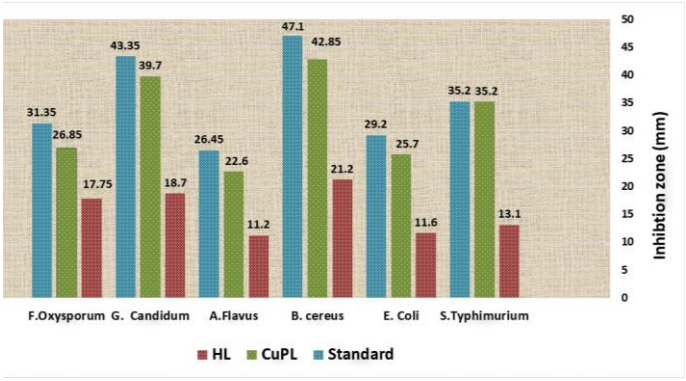

Fig. 10: Relative anti-microbial behavior for the tested compounds at [25 µg/ml] /ml against various strains of bacteria and Fungai.

3.10 Anti-tumor assay

The studied HL ligand [17] and its CuPL chelate have been estimated for its in vitro cytotoxic performance towards human colon [HCT-116; HePG-2; MCF-7] tumor cell lines applying the MTT study. The IC_{50} results for the tested compounds are displayed graphically in (**Figure 11**) also reviewed in (**Table S6**). The obtained results exposed good cytotoxicity of the HL ligand and their Cu(II) complex against both selected cell lines. The HL ligand had higher IC_{50} results towards all carcinoma cell lines than the tested CuPL chelate which specifies the developed cytotoxic performance of CuPL complex than the HL ligand. This might be ascribed to the improved pairing in the chelated ligand as a significance of the chelation with the Cu(II) metal cation. Associated with the reference anti-cancer drug, Doxorubicin, Cu(II) complex has well anti-cancer performance towards all selected cancer cells, however, their performance has been slightly lower than this reference (**Figure 11**). It should be noted that mixed ligand complexes have a key role in biological chemistry because mixed chelation occurs commonly in biological fluids, as millions of potential ligands are likely to compete for metal cation ions in vivo. These create specific structures and have been implicated in the storage and transport of active substances through membranes. In addition, 1,10-Phenanthroline easily forms octahedral complexes with most transition metal cations. 1,10-Phenanthroline behaves as an anti-tumor agent because of its heteroaromatic planar and hydrophobic structure. In addition, this chelating agent shows better anti-tumor activity through chelation with metal cation. This will be more permeable through cell membranes eventually behaving as carriers of anti-tumor agents. This indicated an improvement in the anti-tumor potency upon coordination. The improvement of cytotoxic potency may be attributed to the positive charge of the metal cation increasing the acidity of coordinated ligand that bears protons, causing stronger hydrogen bonds which enhance the biological activity. It seems that changing the coordination sites and the nature of the metal cation has a clear effect on biological activity by altering the binding ability of DNA. Furthermore, the action of the Cu (II) complex is battered at Cu (II) levels in addition to growths only in tumor cells, through the probable proteasome inhibition and apoptosis initiation [52, 53].

Table 5: MIC for the anti-microbial study of the prepared compounds.

Compounds	MIC
Conc.(µg/ml)	CuPL
S.Typhimurium (-ve)	3.50
Escherichia Coli(-ve)	3.75
Bacillus cereus (+ve)	2.75
Aspergillus Flavus	3.75
Getrichm Candidum	3.25
Fusarium Oxysporum	4.5

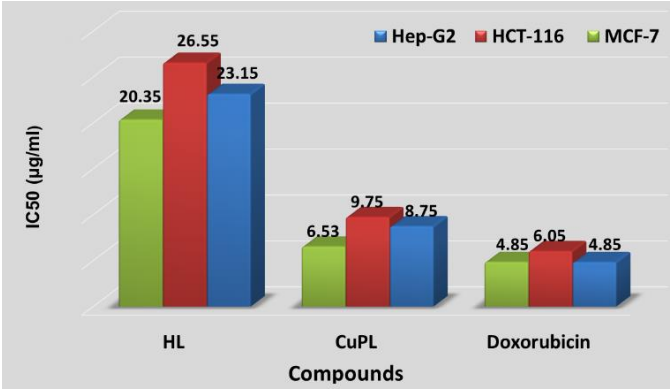

Fig. 11: IC_{50} data for the tested compounds vs examined three cancer cell lines.

Conclusion

Standard processes have been applied to fabrication and investigate HL and its CuPL complex, also characterized through various analytical processes. The observed data exposed the presence of [1 Cu(II): 1 HL: 1 Phen] and recommended the structure for the CuPL complex is [Cu(HL)(Phen)(CH_3COO)].H_2O. The CuPL complex has an octahedral geometry while the (HL & Phen) ligands perform as a monobasic bi-dentate complicated by the N_2 atom of each ligand, based on spectra, analytical, magnetic, and

computational study. The calculated geometrical factors characterize that all atoms on the HL ring's atoms are sitting in the same plane. HOMO–LUMO study and the energy gap have been approved through the recommended study toward the charge distribution ability inside medicinal and in pharmacology. The MEPs plots specify around their zone of Four N_2 atoms have (-ve) impending these are the energetic sites for the coordination. Moreover, biomedical behavior has been offered onto two paths, one of them involved in silico and the second applied in vitro to reinforce the application section. In silico has been applied through MOE docking. All obtained factors or charts indicate the advantage of the Cu(II) chelate in biomedical applications. This hypothesis has been verified currently from in-vitro analysis that explored the anti-microbial and anti-tumor performance of the CuPL complex. Also, an inhibition zone study was applied for the estimation of the anti-microbial analysis. The observed results show that the HL and CuPL compounds have superior anti-microbial activity towards various bacterial and Fungai strains. Finally, the estimated IC_{50} results reinforced the characterized biomedical behavior of Cu (II) chelate toward the examined three cancer cell lines.

CRediT authorship contribution statement:

Ahmed Abu-Dief: Conceptualization, Methodology, Project administration, Supervision. Rafat M. El-Khatib: Investigation, Supervision. Tarek Eldabea: Methodology, Writing – original draft. Aly Abdou: Methodology. Mahmoud Abd El Aleem Ali Ali El-Remaily: Methodology, Supervision

Data availability statement

The data used to support the findings of this study are available from the corresponding author upon request.

Declaration of competing interest

The authors declare that they have no known competing financial interests or personal relationships that could have appeared to influence the work reported in this paper.

Reference

[1] J. H. Al-Fahemi, F. A. Saad, N. M. El-Metwaly, T. A. Farghaly, M. G. ElGhalban, Appl. Organomet. Chem, 31(2017) e3787.
[2] I. Althagafi, N. M. El-Metwaly, M. Elghalban, T. A. Farghaly, A. M. Khedr, Bioinorg. Chem. Appl, 2018 (2018) 1.
[3] H. K. Mahmoud, S. M. Gomha, T. A. Farghaly, H. M. Awad, Polycyclic Aromat. Compd, 41(2021) 1608−1622.
[4] S. O.Alzahrani, A. M.Abu-Dief, K.Alkhamis, F.Alkhatib, T.El-Dabea, M.A.E.A. A. El-Remaily & N. M. El-Metwaly, J. Mol Liq. 332 (2021) 115844.
[5] A. S. Sokolova, O. I. Yarovaya, N. I. Bormotov, L. N. Shishkina, N. F. Salakhutdinov, Med Chem Comm, 9 (2018) 1746.
[6] X. Zou, P. Shi, A. Feng, M. Mei, Y. Li, Transition Met. Chem. 46 (2021) 263.
[7] F. Thomas, Eur. J. Inorg. Chem. 17 (2007) 2379–2404.
[8] T. Basak, K. Ghosh, S. Chattopadhyay, Polyhedron 146 (2018) 81–92
[9] S. Dasgupta, S. Karim, S. Banerjee, M. Saha, K.D. Saha, D. Das, Dalton Trans. 49 (4) (2020) 1232–1240.
[10] A. Ali, N. Abdullah, M.J. Maah, Asian J. Chem, 25 (2013) 3105–3108.
[11] A.O. Sobola, G.M. Watkins, B. Van Brecht, Afr. J. Chem. 67 (2014) 45–51
[12] H. Konaka, L.P. Wu, M. Munakata, T. Kuroda-Sowa, M. Maekawa, Y. Suenaga, Inorg. Chem. 42 (2003) 1928-1934.
[13] A. Schneemann, V. Bon, I. Schwedler, I. Senkovska, S. Kaskel, R.A. Fischer, Flexible metal–organic frameworks, Chem. Soc. Rev., 43 (2014) 6062-6096.
[14] L. Liu, C. Huang, Z.C. Wang, D.Q. Wu, H.W. Hou, Y.T. Fan, Cryst.Eng. Comm, 15 (2013) 7095-7105.
[15] L. Liu, Y.H. Liu, G. Han, D.Q. Wu, H.W. Hou, Y.T. Fan, Inorg. Chim. Acta, 403 (2013) 25-34.
[16] S. Shen, V. Benoy, J.A. Bergman, J.H. Kalin, M. Frojuello, G. Vistoli, W. Haeck, L. Van Den Bosch, A. P. Kozikowski, ACS Chem. Neuro. sci. 7 (2016) 240–258.
[17] A. M. Abu-Dief, R. M. El-Khatib, T. El-Dabea, A. Abdou, F. S. Aljohani, E. S. Al-Farraj, I.O. Barnawi & M. A. E. A. A. A. El-Remaily, J. Mol Liq, 386 (2023)122353.
[18] S. K. Mohamed, A. M. Soliman, M. A. E. A. A. A. El-Remaily, H. Abdel-Ghany, Chem. Sci. J, 7(2013) 1-11.
[19] G. A. Bain, J. F. Berry, Chem. Educ. 85(4)(2008) 532.
[20] J. H. F. Flynn, L. A. Wall, J. Res. Natl. Bur. Stand. A, 70(6) (1966) 487-523.
[21] A.W. Coats, J.P. Redfern, Nature, 201(1964) 68-69.
[22] A. I. Vogel, Quantitative Inorganic Analysis; Longmans: London, (1989) 750.
[23] M. A. A. El-Remaily, N. M. El-Metwaly, T. M. Bawazeer, M. E. Khalifa, T. El-Dabea, A. M. Abu-Dief , Appl. Organomet. Chem, 35(2021) e6370.
[24] A. D. Becke, J. Chem. Phys., 98 (1993) 5648.
[25] A. D. McLean, G. S. Chandler, J. Chem. Phys., 72(1980) 5639-5648.
[26] P. J. Hay, W. R. Wadt, J. Chem. Phys, 82 (1985) 270-83.
[27] S. Mouilleron, M. A. Badet-Denisot, B. Golinelli-Pimpaneau, J. Mol. Biol, 377 (2008) 1174-1185.
[28] N. Colloc'h, L. Gabison, G. Monard, M. Altarsha, M. Chiadmi, G. Marassio, J. Sopkova-de Oliveira Santos, M. El Hajji, B. Castro, J.H. Abraini, T. Prange, Biophys J 95 (2008) 2415-2422.
[29] H.F. El-Shafiy, M. Saif, M. M. Mashaly, S. A. Halim, M. F. Eid, A. Nabeel, R. Fouad, J. Mol. Struct. 1147 (2017) 452-461.
[30] Y. N. Franco, M. Mesa, Int. J. Biol. Macromol. 192 (2021)736-744.
[31] M. Alem, T. Damena, T. Desalegn, M. Koobotse, R. Eswaramoorthy, K. Ngwira, J. Ombito, M. Zachariah, T. Demissie, Front. Chem. 10(2022) 1028957
[32] S. Bhattacharya, A. P. Sherje, J. Drug Delivery Sci. Technol. 60 (2020) 102000.
[33] E. M. Zayed, G. G. Mohamed, H. A. Abd El Salam, Inorgan. Chem. Comm, 147 (2023)110276.
[34] J. Mosmann, J. Immunol. Methods 65(1983) 55-63.
[35] K. M. Ibrahim, R. R. Zaky, E. A. Gomaa, L. A. Yasin, J. Mol. Struct, 1101(2015) 124-138.
[36] G.A.A. Al-Hazmi, K.S. Abou-Melha, N.M. El-Metwaly, I. Althagafi, Rania Zaky, F. Shaaban, J Inorg Organomet Polym 30 (2020)1519-1536.
[37] V. P. Singh, S. Singh, D. P. Singh, J. Enzyme Inhib. Med. Chem, 27(2012) 319-329.
[38] Y. Futami, Y. Ozaki, Y. Hamada, M. J. Wojcik, Y. Ozaki, Chem. Phy. Lett, 482(4-6) (2009) 320-324
[39] M. A. E. A. A. A.El-Remaily, A. M.Soliman, M. E.Khalifa, N. M.El-Metwaly, A. Alsoliemy, T. El-Dabea, A. M. Abu-Dief, Appl Organomet Chem, 36(2) (2022) e6320
[40] M. Gaber, H. A. El-Ghamry, M. A. Mansour, J. Photochem. Photobiol. A, 354(2018)163-174.
[41] K. M. Takroni, T. A. Farghaly, M. F. Harras, & H. A. El-Ghamry,. Appl. Organomet. Chem, 34(10)(2020) e5860.
[42] F. A. Saad, H. A. El-Ghamry, M. A. Kassem, Appl. Organomet. Chem, 33(7)(2019) e4965.

[43] A. M. Abu-Dief, N. M. El-Metwaly, S. O. Alzahrani, F. Alkhatib, H. M. Abumelha, T. El-Dabea, & M. A. E. A. A. El-Remaily, Res. Chem. Inter. 47 (2021) 1979-2002.
[44] Y. A. A. Alghuwainem, H. M. Abd El-Lateef, M. M. Khalaf, A. A. Amer, A. A. Abdelhamid, A. A. Alzharani, A. Alfarsi, S. Shaaban, M. Gouda, A. Abdou, Inter. J. Mol Sci. 23(24)**(**2022), 15614; .
[45] M. d. Azharul Arafath, F. Adam, M. B. K. Ahamed, M. R. Karim, M.d. N. Uddin, B. M. Yamin, A. Abdou, J . Mol. Struct, 1278(2023) 134887.
[46] N.A. A. Elkanzi, A.M. Ali, M. Albqmi, A. Abdou, Appl. Organomet. Chem, 36(11) (2022) e6868.
[47] H. A. K. Kyhoiesh, K. J. Al-Adilee, Inorganica Chim Acta, 555(2023) 121598.
[48] N. A.A. Elkanzi, H. Hrichi, H. Salah, M. Albqmi, A. M. Ali, A. Abdou, Polyhedron, 230 (2023) 116219.
[49] H. Hrichi, N. A. A. Elkanzi, A. M. Ali, A. Abdou, Res. Chem. Intermed, 49(2023) 2257–2276.
[50] M. d. Azharul Arafath, F. Adam, M. B. K. Ahamed, M. R. Karim, M.d. N. Uddin, B. M. Yamin, A. Abdou, J . Mol. Struct, 1278(2023)134887,
[51] T. Damena, M. B. Alem, D. Zeleke, T. B. Demissie, T. Desalegn, J. Mol. Struct. 1280(2023)134994.
[52] Y. Anjaneyulu, R. P. Rao, Synth. React. Inorg. Met. Org. Chem. 16 (1986) 257-272.
[53] M. Gaber, S. K. Fathalla, H. A. El-Ghamry, Appl. Organomet. Chem, 33(4) (2019) e4707.